ORNL/CP-95750

NANOINDENTATION OF SOFT FILMS ON HARD SUBSTRATES: EXPERIMENTS AND FINITE ELEMENT SIMULATIONS

CONF-97120/--

G.M. PHARR*, A. BOLSHAKOV**, T.Y. TSUI*, and JACK C. HAY***
* Department of Materials Science, Rice University, 6100 Main St., Houston, TX 77005-1892
** Baker Hughes Inteq, P.O. Box 670968, Houston, TX 77267-0968
*** Metals and Ceramics Division, Oak Ridge National Laboratory, Oak Ridge, TN 37831

ABSTRACT

Experiments and finite element simulations have been performed to examine errors in the measurement of hardness and elastic modulus caused by pile-up when soft films deposited on hard substrates are tested by nanoindentation methods. Pile-up is exacerbated in soft-film/hard-substrate systems by the constraint imposed on plastic deformation in the film by the relatively non-deformable substrate. To experimentally examine pile-up effects, soft aluminum films with thicknesses of 240, 650, and 1700 nm were deposited on hard soda-lime glass substrates and tested by nanoindentation techniques. This system is attractive because the elastic modulus of the film and the substrate are approximately the same, but the substrate is harder than the film by a factor of about ten. Consequently, substrate influences on the indentation load-displacement behavior are manifested primarily by differences in the plastic flow characteristics alone. The elastic modulus of the film/substrate system, as measured by nanoindentation techniques, exhibits an increase with indenter penetration depth which peaks at a value approximately 30% greater than the true film modulus at a penetration depth close to the film thickness. Finite element simulation shows that this unusual behavior is caused by substrate-induced enhancement of pile-up. Finite element simulation also shows that the amount of pile-up increases with increasing penetration depth, and that the pile-up geometry depends on the work-hardening characteristics of the film. Because of these effects, nanoindentation techniques overestimate the true film hardness and elastic modulus by as much as 68% and 35%, respectively, depending on the work-hardening behavior of the film and the indenter penetration depth. The largest errors occur in non-work-hardening materials at penetration depths close to the film thickness, for which substrate-induced enhancement of pile-up is greatest.

INTRODUCTION

Nanoindentation is a widely used technique for characterizing mechanical properties at the micron and sub-micron scales [1-5]. Nanoindentation techniques have proven particularly useful in measuring the hardness, H, and elastic modulus, E, of thin films [6-11]. However, when the film is very thin, e.g., less than about a micron, accurate measurements are sometimes difficult to achieve because of substrate influences on the indentation deformation behavior. As a result, numerous experimental and theoretical investigations have addressed the issue of substrate effects and what can be done to obtain substrate-independent measurements of thin film mechanical properties [10-15].

Many thin film systems are comprised of soft films on hard substrates. This is particularly common, for instance, in the semiconductor industry, where films of aluminum, gold and copper are often deposited on silicon (H = 12 GPa), germanium (H = 10 GPa), glass (H = 5-8 GPa) and ceramic substrates (H = 10-40 GPa). The hardness of these films is usually in the range 0.1-1 GPa, making them at least an order of magnitude softer than the materials on which they are deposited. One important consequence is that when an indentation is made, there is a tendency for material to pile-up around the hardness impression to a much greater degree than it would in a monolithic material, due to the constraint imposed on plastic deformation in the film by the relatively non-deformable substrate [6,16,17]. Since techniques for analyzing nanoindentation

data do not account for the extra contact area produced by the pile-up [18-21], the enhancement of pile-up in soft films on hard substrates has important consequences for film property measurement accuracy. In particular, the hardness and the elastic modulus are determined from nanoindentation load-displacement data using the relations [2]:

$$H = \frac{P_{max}}{A} \tag{1}$$

and

$$E = \left(1 - \nu^2\right)\left[\frac{2}{\sqrt{\pi}}\beta\frac{\sqrt{A}}{S} - \frac{1-\nu_i^2}{E_i}\right]^{-1} \tag{2}$$

where, P_{max} is the peak indentation load, A is the projected indentation contact area, β is a constant depending on the indenter geometry, S is the experimentally measured contact stiffness, ν is Poisson's ratio of the specimen, and ν_i and E_i are Poisson's ratio and the elastic modulus of the indenter. Thus, the accuracy with which the hardness and modulus can be measured depends on how well the contact area is known, since the area appears explicitly in both equations. In most nanoindentation methods [2,3], the contact area is measured by evaluating an empirically-determined indenter shape function at the contact depth, h_c, where the contact depth has been estimated from the indentation load-displacement data using a procedure based on a solution for the indentation of an elastic half-space by a rigid punch [22]. However, since the solution is only elastic, contributions due to plasticity and pile-up are inherently ignored, and this leads to an underestimation of the contact area and thus an overestimation of the hardness and modulus in materials which pile-up [20,21].

In order to gain a better understanding of the importance of pile-up in nanoindentation mechanical property measurement of soft films on hard substrates, an experimental investigation was undertaken to explore the pile-up behavior of a model material system. Finite element simulations were also performed to gain physical insight into the pile-up behavior as well as to explore the importance of the work-hardening characteristics of the film. In this paper, important observations and their implications for nanoindentation mechanical property measurement accuracy are presented and discussed.

EXPERIMENTAL PROCEDURE

The model system used in the investigation was high purity aluminum deposited on glass. In addition to a large difference in hardness (the hardness of the film is in the range 0.5-1.0 GPa while that for the substrate is 7.0 GPa), an equally important consideration in the choice of the system was the similarity of the elastic moduli of the two components. The modulus of aluminum is 70 GPa, while that for the glass used in the study is 57 GPa, as measured by nanoindentation methods. The fact that the moduli are similar minimizes the role that a film/substrate modulus difference would play in determining the indentation load-displacement behavior, thus simplifying the interpretation of results. The films were sputter-deposited to three different thicknesses, t_f = 240 nm, 650 nm, and 1700 nm, and indented to various penetration depths, h, with a sharp Berkovich diamond indenter. The load-displacement data obtained at each depth were analyzed by the method of Oliver and Pharr [2] using β = 1.034, ν_i = 0.07, E_i = 1141 GPa, and ν = 0.34 to determine the apparent contact area, hardness, and elastic modulus. The quantities measured in this way, which do not account for pile-up influences, will be referred to as A_{nano}, H_{nano}, and E_{nano}.

The larger hardness impressions were also imaged in a high resolution scanning electron microscope (SEM) to determine the actual contact areas, A_{actual}, taking care to include the pile-up in the contact area determination. The actual areas were measured by tracing a digital image of each indentation along the contact edge and computing the area enclosed inside the figure. Values

DISCLAIMER

DISCLAIMER

Portions of this document may be illegible electronic image products. Images are produced from the best available original document.

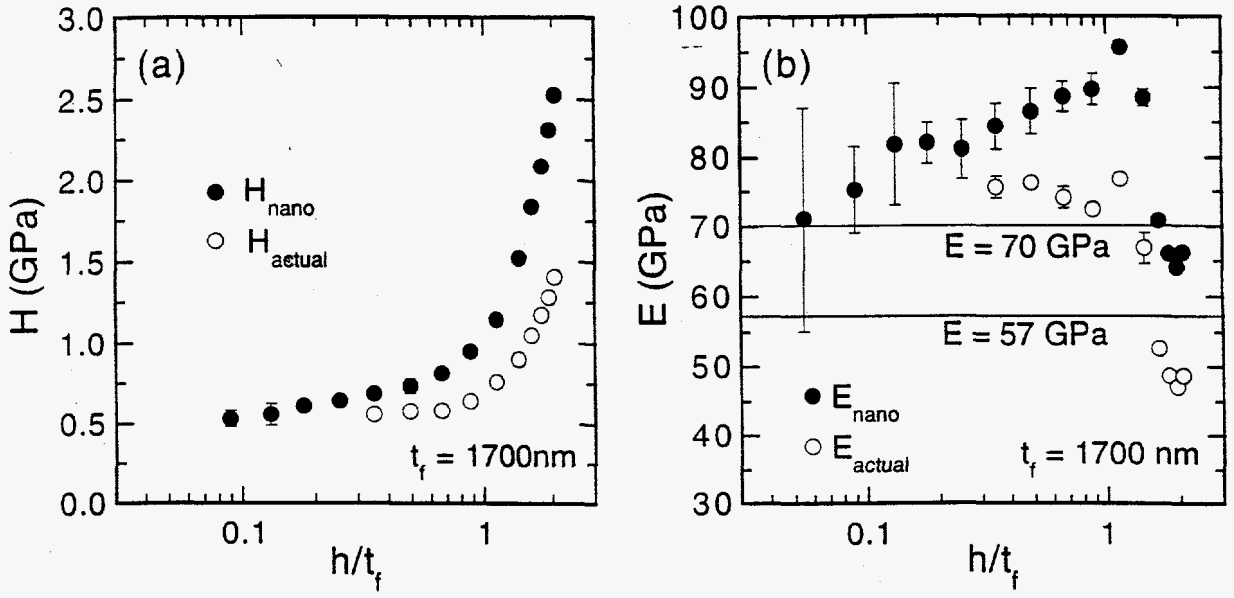

Fig. 1. Hardness and elastic modulus of the 1700 nm aluminum film on a glass substrate.

of A_{actual} measured in this way were used in Eqns. 1 and 2 to provide a second measure of the hardness and modulus, H_{actual} and E_{actual}. Note that by definition, H_{actual} is the true hardness. Thus, any deviations of H_{nano} from H_{actual} must be attributed to inaccuracies in the procedure by which contact areas are deduced from the indentation load-displacement data. Quantitative measures of the characteristics of the pile-up such as the pile-up height, h_{pu}, were determined by atomic force microscopy (AFM).

EXPERIMENTAL RESULTS

Fig. 1 summarizes the results of hardness and modulus measurements for the 1700 nm film. The thickness of this film makes it convenient for measurements at penetration depths less than the film thickness ($h \leq t_f$). The filled symbols show the dependencies of H_{nano} and E_{nano} on the penetration depth normalized with respect to the film thickness, h/t_f. Each data point is an average from at least five indentations, with scatter bars indicating one standard deviation. The behavior of the composite hardness of the film/substrate system in Fig. 1a is reasonable. At small depths, the hardness tends towards a limiting value of about 0.5 GPa, presumably the hardness of the film, but at large depths, the hardness increases markedly, consistent with a substrate hardness of 7.0 GPa. Most of the increase occurs at penetration depths close to the film thickness. The behavior of the elastic modulus, on the other hand, is quite different. At small depths, E_{nano} is close to the expected film modulus, 70 GPa, but at larger depths, E_{nano} shows an unexpected increase to a peak value of about 90 GPa at a depth close to the film thickness. Following the peak, there is an sharp decrease in the modulus. The increase in modulus to values above 70 GPa is especially surprising given that modulus of the substrate, 57 GPa, is smaller that of the film.

Careful examination of the contact impressions in the films revealed that the higher than expected elastic modulus in Fig. 1b originates from substrate-induced enhancement of pile-up. Three SEM images illustrating the nature of the pile-up are shown in Fig. 2. The first two indentations were made in the 1700 nm film at $h/t_f = 0.18$ and 1.43, and the third in the 240 nm film at $h/t_f = 9.96$. Pile-up of various forms is visible in all three SEM images. One notable feature of the pile-up is the non-uniform distribution around the contact periphery; pile-up is most extensive near the centers of the edges of the indentation but virtually absent at the corners, as verified by AFM surface profiles. Another notable feature is the change in the shape of the

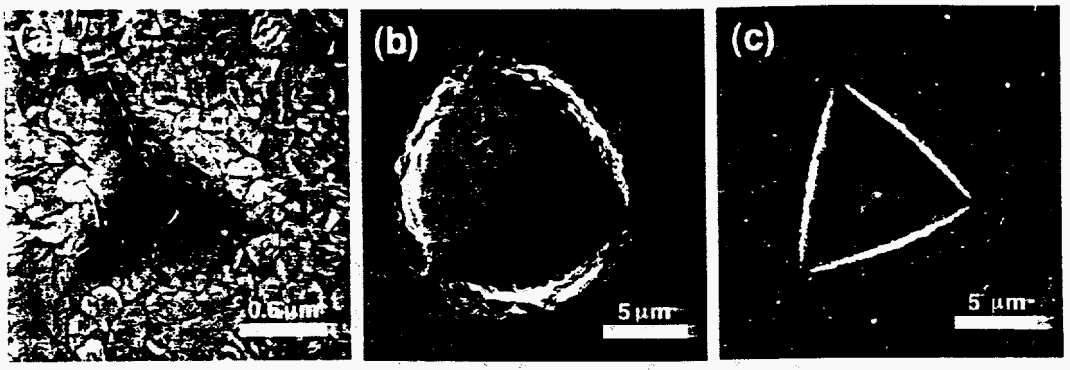

Fig. 2. SEM images of indentations: (a) $h/t_f = 0.18$; $t_f = 1700$ nm; (b) $h/t_f = 1.43$; $t_f = 1700$ nm; and (c) $h/t_f = 9.96$; $t_f = 240$ nm.

contact geometry at the contact periphery from triangular at small depths (Fig. 2a) to roughly circular at the contact depths close to the film thickness (Fig. 2b) and then to triangular again at larger depths (Fig. 2c). The change is due to differences in the form and distribution of pile-up.

To provide a quantitative measure of the pile-up, the pile-up heights, h_{pu}, were determined by AFM examination. The pile-up height is defined as the vertical distance between the undeformed surface and the peak of the pile-up at the center of a face of the hardness impression. The dependence of h_{pu}/h on h/t_f is shown in Fig. 3. It is evident that the amount of pile-up is small at small indentation depths, in accordance with the behavior of monolithic, annealed aluminum [23], but rises to a distinct maximum at depths close the film thickness before falling at large depths. At the peak, the height of the pile-up is approximately 50% of the indentation depth. Apparently, as the indenter approaches the substrate, plastic flow in the film is restricted by the relatively non-deformable substrate in a manner which causes the soft film material to flow preferentially toward the surface and enhance pile-up. The amount of pile-up decreases when the indenter penetrates through the film because the glass substrate sinks in during indentation rather than piling up [23].

The fact that there is significant substrate-induced pile-up in the aluminum film means that the contact areas deduced from the nanoindentation load-displacement data are in error, which in turn produces errors in the nanoindentation hardness and elastic modulus. To quantify the magnitude of the errors, the actual contact areas of indentations in the 1700 nm film measured from SEM images are plotted in Fig. 4 as A_{actual}/A_{nano} vs. h/t_f. The results show that there is indeed an increase in contact area due to pile-up and that the true contact area is as much as 80% greater than that derived from the nanoindentation data analysis procedures. Clearly, this must be accounted for if accurate measurements of E and H are to be obtained; otherwise, errors as large as 80% in the hardness and 34% in the elastic modulus could result (see Eqns. 1 and 2). For purposes of comparison, the hardnesses and elastic moduli computed from Eqns. 1 and 2 using the actual contact areas are plotted as open circles in Fig. 1. Some of the very small indentations could not be imaged with sufficient resolution to make accurate area measurements and are not included in the plot. The data show that for indentation depths less than the film thickness, use of the actual contact area reduces the measured moduli to relatively constant values in the range 72-77 GPa, i.e., much closer to what would be expected. In addition, the hardness is reduced by as much as a factor of 1.8, depending on the indentation depth. An interesting feature of the data in Fig. 1a is the relative constancy of H_{actual} for indentation depths less the film thickness. Thus, the approximately factor of two increase observed in H_{nano} at depths less than the film thickness is not real but an artifact related to pile-up.

As detailed elsewhere [6,24], the abrupt decrease in elastic modulus at penetration depths greater than the film thickness observed in Fig. 1b has two separate origins. First, the modulus of the substrate, 57 GPa, is approximately 20% smaller than the film, so a small decrease is naturally expected. However, this by itself can explain neither the abruptness of the decrease nor

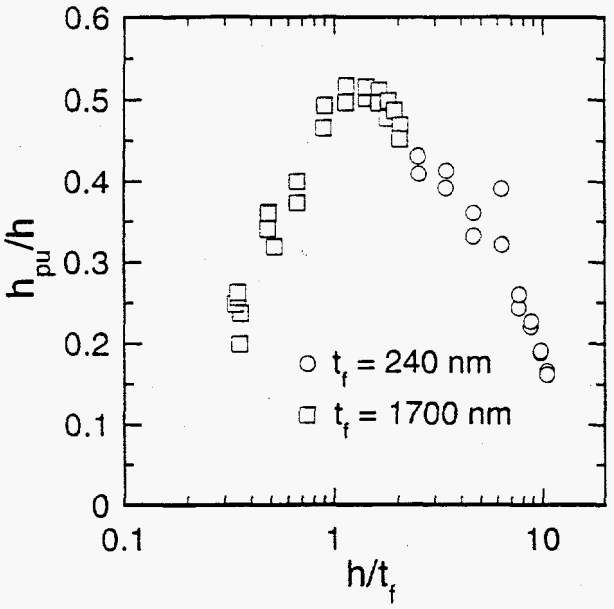

Fig. 3. Indentation depth dependence of h_{pu}/h for the 1700 nm film.

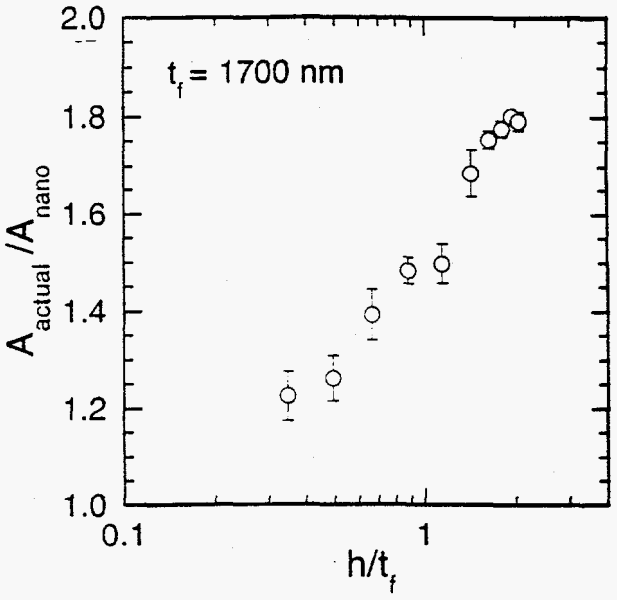

Fig. 4. Indentation depth dependence of A_{actual}/A_{nano} for the 1700 nm film.

the reduction in E_{actual} to values less than 57 GPa. Rather, the lower than expected modulus is an artifact caused by the curve fitting procedures used to estimate the unloading stiffness. Specifically, glass recovers elastically during unloading to a much greater degree than aluminum [23]. As a result, during the unloading of an indentation which has penetrated through the film into the glass, indenter contact with the aluminum is lost in the early stages of unloading, and the displacements recovered during the lower portion of the unloading curve are determined by elastic recovery of the glass only. This changes the shape of the unloading curve in a way that makes it not fit well by a power-law fitting relation. The net effect is that unloading stiffness derived from a power-law fit of the unloading curve is underestimated, which translates via Eqn. 2 to an underestimation of the elastic modulus. One might suspect that this problem could be avoided by using a smaller portion of the unloading data to determine the contact stiffness. However, aluminum films exhibit significant creep during indentation, and the creep displacements produce other errors in the contact stiffness when only small portions of unloading data are used in curve fitting [24].

A more effective way to avoid the underestimation of the contact stiffness when the indenter penetrates through the film into the substrate is through the use of continuous stiffness measurement techniques [2]. In these techniques, a small force oscillation is imposed on the load signal, and the stiffness is measured continuously during loading by analyzing the displacement signal with a phase sensitive amplifier. With this technique, the indenter never loses contact with the film, and because the stiffness measurement can be made on a relatively short time scale, problems caused by creep are minimized. Nanoindentation modulus measurements for the 650 nm film made using continuous stiffness measurement techniques are shown in Fig. 5. As in Fig. 1b, the pile-up induced increase in E_{nano} with increasing penetration depth is evident (although the magnitude of the peak is smaller than that in Fig. 1b), but the abrupt drop in modulus at depths greater than the film thickness is completely absent. Continuous stiffness measurement thus offers distinct advantages when the properties of soft-film-on-hard-substrate systems are to be explored at indentation depths greater than the film thickness.

FINITE ELEMENT SIMULATION PROCEDURE

Finite element simulations were conducted to gain insight into the experimental results and

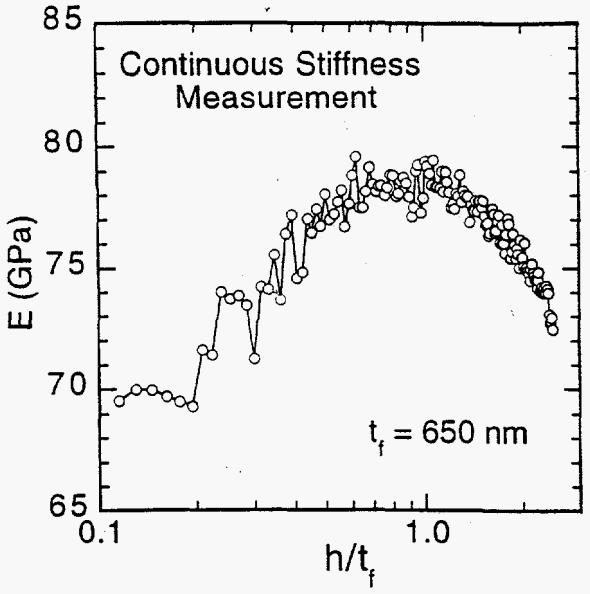

Fig. 5. Elastic modulus of the 650 nm film determined by continuous stiffness measurement techniques.

develop a better understanding of the role played by work hardening on the indentation behavior. Elastic/plastic indentation was simulated using the axisymmetric capabilities of the ABAQUS finite element code. The indenter was modeled as a rigid cone with semi-vertical angle $\phi = 70.3°$, which gives the same area-to-depth ratio as the Berkovich indenter used in the experiments. The specimen was modeled as a cylinder 100,000 nm high and 100,000 nm in radius with a 240 nm thin film on its surface. The finite element mesh was similar to one employed in previous studies [20,21]. Near the contact, very fine elements were used to achieve precise measurements of contact radii and contact areas. Away from the contact, a progressively coarser mesh was employed both at the surface and in the interior of the specimen. The interface between the indenter and the specimen was assumed to be frictionless.

To simplify the interpretation of results, the film and substrate were assigned the same elastic properties given by Young's modulus E = 70 GPa and Poisson's ratio $\nu = 0.34$. The substrate was modeled as an elastic-perfectly-plastic solid with yield stress $\sigma_y = 3.105$ GPa. This yield stress is associated with a substrate hardness of 6.41 GPa, similar to glass. Two different film materials were simulated characterized by different linear work-hardening rates $\eta = d\sigma/d\varepsilon$. In one, elastic perfectly-plastic behavior was assumed ($\eta = 0$), and in the other, a moderate rate of work hardening, $\eta = 10\sigma_y$, which increases the flow stress by a factor of two at 10% plastic strain, was employed. The yield stresses of the films, $\sigma_y = 0.265$ GPa for the elastic-perfectly-plastic material ($\eta = 0$) and $\sigma_y = 0.120$ GPa for the work-hardening-plastic material ($\eta = 10\sigma_y$), were chosen to give the two film materials the same inherent hardness, H = 0.69 GPa, which is similar to that of aluminum.

Simulations were conducted to a variety of penetration depths, but concentrating on depths less than the thickness of the film. The output of the finite element simulations included indentation load-displacement curves, the shapes of contact impressions, and the geometries of plastic zones. As in the data obtained in experiments, the finite element load-displacement curves were analyzed to determine the hardness and elastic modulus using the Oliver-Pharr data analysis procedures [2]. To implement the analysis, the upper 10% of the unloading curve was fit to a power law relation, and the curve fitting parameters were used to determine the unloading stiffness S=(dP/dh) at the maximum depth. The Oliver-Pharr method was then applied to determine the contact depth and contact area using $\varepsilon = 0.75$ and the indenter shape function for a perfect cone, $A = \pi d^2 \tan^2\phi$ ($\phi = 70.3°$). Using values of A_{nano} derived in this way, H_{nano} and E_{nano} were computed using Eqns. 1 and 2. In addition, the actual contact areas A_{actual} were determined by direct examination of the finite element mesh and used to determine H_{actual} and E_{actual}, again by means of Eqns. 1 and 2. Unless otherwise noted, the contact areas used in this

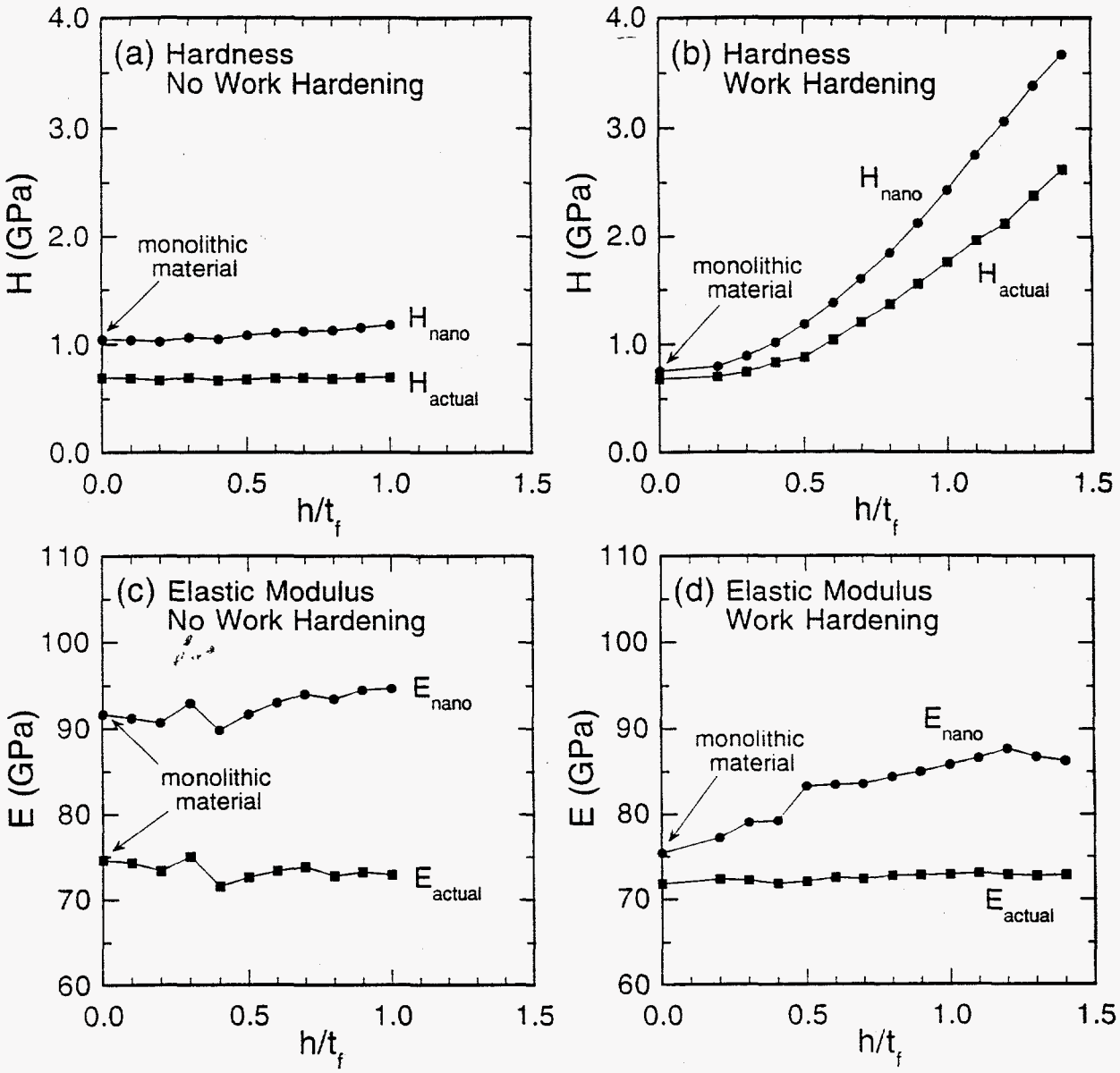

Fig. 6. Hardness and elastic modulus determined by finite element simulation for non-work-hardening ($\eta = 0$) and work-hardening ($\eta = 10\sigma_y$) aluminum films.

work are those obtained after the indenter was withdrawn from the material.

FINITE ELEMENT RESULTS

The depth dependence of the hardness and elastic modulus observed in the finite element simulations is shown in Fig. 6. Only penetration depths up to approximately the film thickness are included since numerical difficulties caused by large strains in some of the elements were encountered at larger depths. The results show that when there in no work hardening in the film (Figs. 6a and 6c), all of the hardnesses and elastic moduli are essentially independent of the penetration depth. Moreover, the value of H_{actual} is in good agreement with the monolithic material (H = 0.69 GPa), and the value E_{actual} is in good accord with the elastic modulus used as input in the simulations (E = 70 GPa). However, as in the case of the experimental data, H_{nano} and E_{nano} are larger than H_{actual} and E_{actual}, presumably due to pile-up influences not accounted

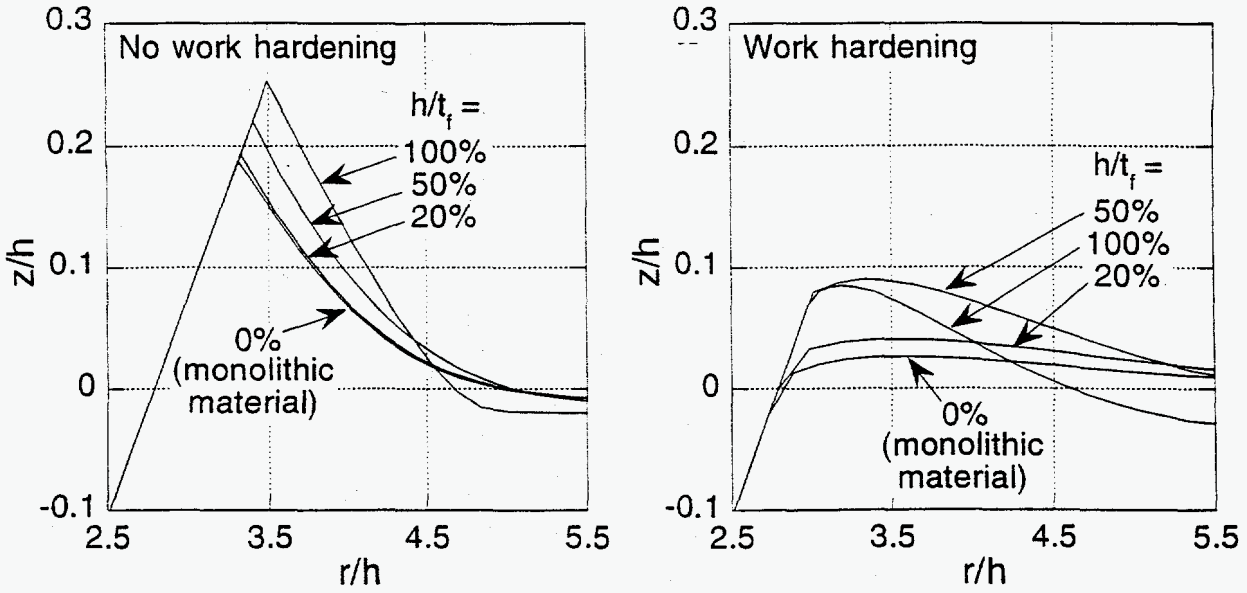

Fig. 7. Indentation pile-up profiles showing the contact geometry with the indenter under load.

for in the nanoindetation data analysis procedures. The hardness is overestimated by as much as 68% and the modulus by 35%. The relative constancy of the actual hardness, even at large penetration depths, is somewhat surprising given that the substrate is much harder than the film. This behavior was also observed in the experimental data.

The behavior of the work-hardening material, Figs. 6b and 6d, is distinctly different. Rather than being constant, H_{actual} and H_{nano} both increase with increasing penetration depth, starting from a value close to the hardness of the monolithic material (H = 0.69 GPa). The rate of increase is greater for H_{nano}, for which the hardness increases by more than a factor of 5 at h/t_f = 1.4. While E_{nano} also shows an increase, values of E_{actual} are relatively constant near 70 GPa. The constancy of E_{actual} for both the work-hardening and non-work-hardening materials at a value close to that used as input in the finite element simulations attests to the validity of Eqn. 2 in the measurement of elastic modulus of soft-film-on-hard-substrate systems.

Many of the observations in Fig. 6 can be understood by examining the indentation pile-up behavior and how it varies with indenter penetration into the film. To illustrate this, Fig. 7 presents cross-sectional indentation pile-up profiles showing the geometry of the contact under load, and in Fig. 8, the pile-up heights after the indenter has been unloaded are summarized. In order to facilitate comparison, the r and z coordinates in the plots of Fig. 7 have been normalized with respect to the depth of penetration, and in Fig. 8, values of h_{pu}/h obtained from monolithic material simulations are used for $h/t_f = 0$ (i.e., $t_f = \infty$).

Examination of Figs. 7 and 8 shows that the pile-up behavior of the work-hardening and non-work-hardening materials is very different. In general, pile-up is much more extensive when the material does not work harden, consistent with observations for monolithic materials [20,21]. For both types of materials, the amount of pile-up increases with increasing depth, presumably due to substrate constraint on plastic flow in the film. The finite element simulations thus show that the hard substrate does indeed enhance pile-up in the film, with the relative amount of pile-up increasing with penetration depth, at least at depths up to the film thickness, consistent with the experimental observations shown in Fig. 3. It is notable, however, that the relative increases in pile-up are much greater for the work-hardening film because the pile-up heights are much smaller at small penetration depths.

The degree to which the enhancement of pile-up leads to an underestimation of the actual contact area in nanoindentation measurement procedures is shown in Fig. 9, where values of A_{actual}/A_{nano} from the finite element simulation data are plotted as a function of normalized

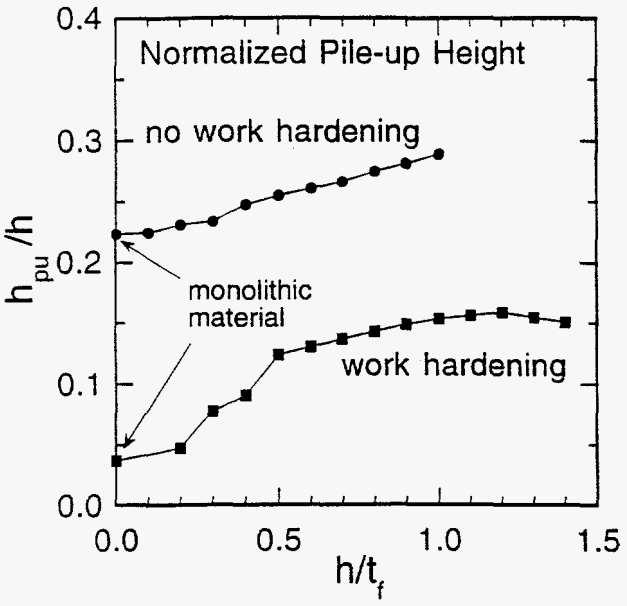

Fig. 8. Indentation depth dependence of h_{pu}/h observed in finite element simulations.

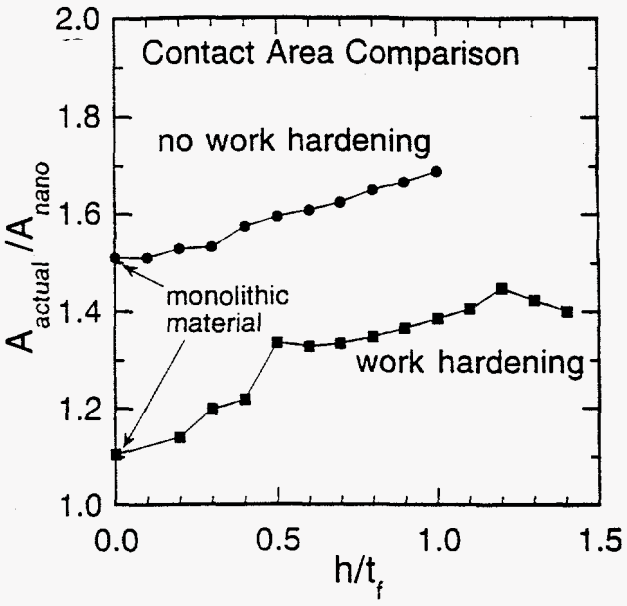

Fig. 9. Indentation depth dependence of A_{actual}/A_{nano} observed in finite element simulations.

penetration depth. When there is no work hardening in the film, the actual contact area is 50-70% greater than that predicted by the nanoindetation data analysis. Work hardening reduces the difference in A_{actual} and A_{nano} to as little as 10% at small depths, but the difference increases to a value of about 45% at a penetration depth slightly greater than the film thickness. Of course, the difference in the two areas is what leads to the overestimation of H_{nano} and E_{nano}.

Physical insight into the differences in the pile-up behavior of the work-hardening and non-work-hardening materials can be gained by examining the plastic zones formed at the hardness impressions. The development of the plastic zones is illustrated in Fig. 10, which shows the plastic zone shapes at penetration depths of 10, 20, 50, 90, and 100% of the film thickness. The behavior of the non-work-hardening material is shown on the left side of the figure. For the non-work-hardening film, the plastic zone at shallow penetration depths (h/t_f = 10%) extends a little more than half way through the film and has a surface dimension of approximately twice the contact radius. As penetration proceeds, the zone grows both vertically and horizontally, but before the penetration depth has reached 20% of the film thickness, the zone extends vertically all the way through the film, terminating at the film substrate interface. Further penetration results in horizontal spreading of the zone in the film, but plastic deformation never commences in the substrate. Apparently, substrate constraint causes film material to flow preferentially to the surface and enhance pile-up.

The work-hardening material, shown on the right-hand side of Fig. 10, exhibits essentially the same characteristics with two notable exceptions. First, as in the case of monolithic materials [21,25], work hardening produces a plastic zone which penetrates much deeper into the material at a given indenter penetration depth. Consequently, the interaction of the plastic zone with the substrate occurs much earlier in the indentation process, so that substrate-induced effects on pile-up are greater at small depths (see Fig. 8). Second, because of the hardening in the film, the stress in the substrate grows to values at which it can yield. For the material examined in this study, substrate yielding occurs after the film is penetrated to a depth of about 90%. Further penetration expands the plastic zones in both the film and the substrate.

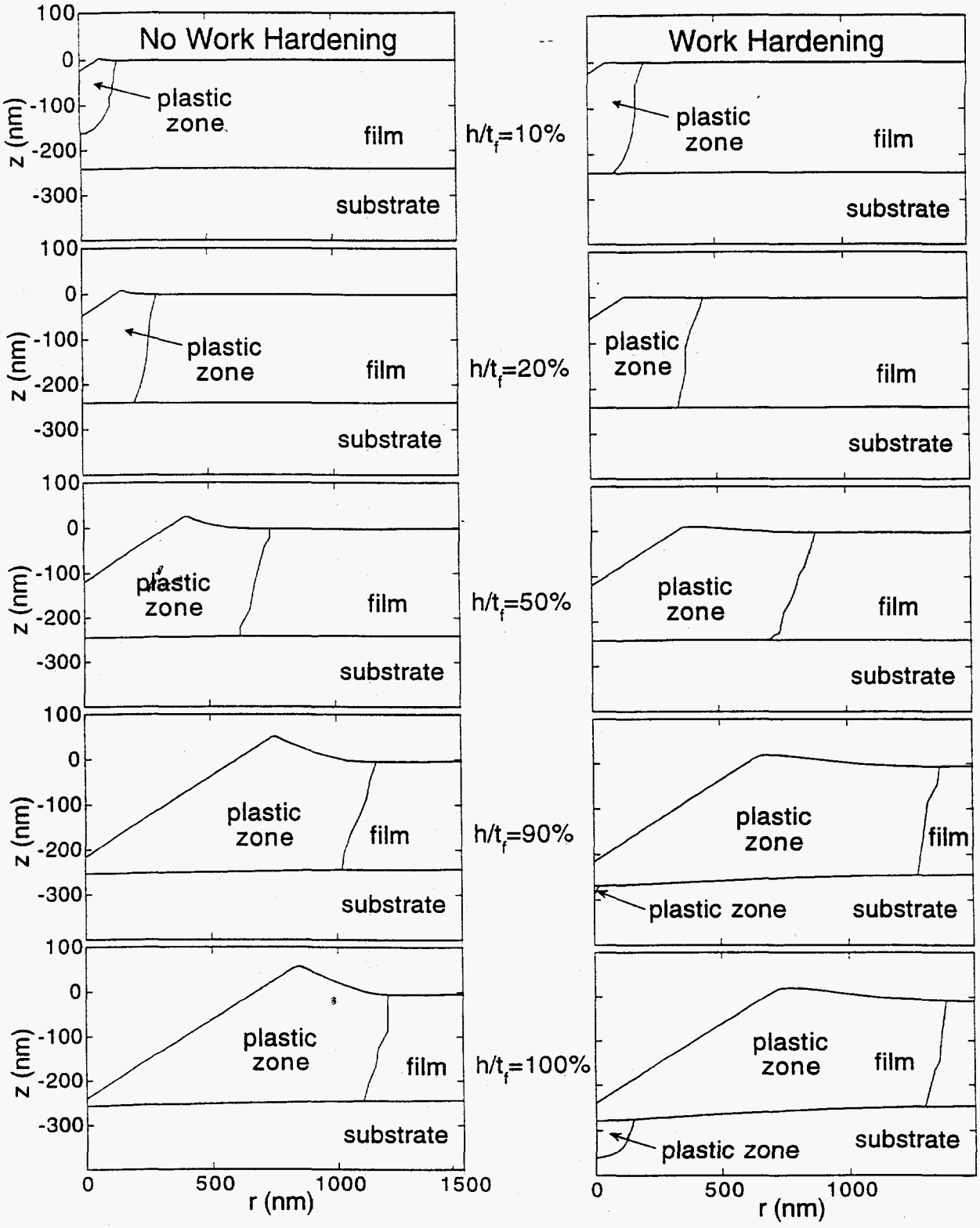

Fig. 10. Plastic zone development observed in finite element simulations.

COMPARISON OF FINITE ELEMENT AND EXPERIMENTAL RESULTS

Before concluding, it is instructive to compare certain aspects of the behavior observed in the finite element simulations with the experimental results. A direct quantitative comparison is not particularly meaningful, since different indenters were used (conical for the FEM simulations and Berkovich for the experiments) and the elastic modulus of the film and substrate in the experimental system were not perfectly matched (70 GPa for the film vs. 57 GPa for the substrate). Nevertheless, certain general trends in the experimental and finite element results are worthy of examination and can be used to comment on the influences of the work-hardening characteristics of the film on the experimental results.

The data in Fig. 3 show that the amount of pile-up in the experimental system, as characterized by the pile-up height, is relatively small at small penetration depths and increases to a value which peaks at a penetration depth in the range of one to two film thicknesses. The increase in pile-up height is also observed in the FEM simulations for both the work-hardening and non-work-hardening materials (Fig. 8), and the associated increase in A_{actual}/A_{nano} (Fig. 9) is directly responsible for the experimental increases of E_{nano} to values greater than 70 GPa in Fig. 1b. It is notable, however, that only for the work-hardening material is the amount of pile-up in Fig. 8 small at small depths and thus consistent with the experimental observations. Based on this, one might conclude that there is at least a moderate amount of work hardening in the film, as is often observed for sputtered aluminum. However, the issue becomes clouded when one compares the actual experimental hardnesses in Fig. 1a with the actual finite element hardnesses of Fig. 6a and 6b. Specifically, for the experimental system, values of H_{actual} at penetration depths less than the film thickness are relatively constant, while in the finite element simulations, depth independent values of H_{actual} are observed only if the material does not work harden. Thus, comparison of the experimental and finite element results reveals a discrepancy concerning the work-hardening behavior of the film. The source of this discrepancy has not yet been identified, but it is conceivably related to details of the work-hardening behavior which cannot be accounted for by the assumption of simple linear work hardening.

CONCLUSIONS

Experimental studies and finite element simulations show that indentation pile-up in soft aluminum films is significantly enhanced when the films are deposited on hard glass substrates. Substrate-induced enhancement of pile-up increases the indentation contact area above what is observed in monolithic aluminum, and is greatest at indentation penetration depths close to the film thickness. Because methods for measuring mechanical properties by nanoindentation do not account for pile-up, the contact area is underestimated, and this produces errors in the measured hardness and elastic modulus. One consequence is that the elastic modulus of the film/substrate system appears to increase with indenter penetration depth to a value which peaks at a depth close to the film thickness. Finite element simulations show that nanoindentation techniques overestimate the true film hardness and elastic modulus by as much as 68% and 35%, respectively, depending on the penetration depth and the work-hardening behavior of the film. The largest errors occur in non-work-hardening materials at penetration depths close to the film thickness, for which substrate-induced enhancement of pile-up is greatest.

ACKNOWLEDGMENTS

This research was sponsored by the Division of Materials Sciences, U.S. Department of Energy, under contract DE-AC05-96OR22464 with Lockheed Martin Energy Research Corp., and through the SHaRE Program under contract DE-AC05-76OR00033 with Oak Ridge Associated Universities.

REFERENCES

1. G.M. Pharr and W.C. Oliver, MRS Bulletin **17**, 28 (1992).
2. W.C. Oliver and G.M. Pharr, J. Mater. Res. **7**, 1564 (1992).
3. M.F. Doerner and W.D. Nix, J. Mater. Res **1**, 601 (1986).
4. J.L. Loubet, J.M. Georges, O. Marchesini, and G. Meille, J. Tribology **106**, 43 (1984).
5. J.B. Pethica, R. Hutchings, and W.C. Oliver, Philos. Mag. A **48**, 593 (1983).
6. T.Y. Tsui, W.C. Oliver, and G.M. Pharr, Mater. Res. Soc. Symp. Proc. **436**, 207 (1997).
7. W.C. Oliver, C.J. McHargue, and S.J. Zinkle, Thin Solid Films **153**, 185 (1987).
8. W.C. Oliver and C.J. McHargue, Thin Solid Films **161**, 117 (1988).
9. M.F. Doerner, D.S. Gardner, and W.D. Nix, J. Mater. Res. **1**, 845 (1987).
10. W.R. LaFontaine, B. Yost, and C.-Y. Li, J. Mater. Res. **5**, 776 (1990).
11. D. Stone, W.R. LaFontaine, P. Alexopoulos, T.W. Wu, and C.-Y. Li, J. Mater. Res **3**, 141 (1988).
12. D.S. Stone, J. Electronic Packing **112**, 41-46 (1990).
13. P.J. Burnett and D.S. Rickerby, Thin Solid Films **148**, 41-50 (1987).
14. P.J. Burnett and D.S. Rickerby, Thin Solid Films **148**, 51-65 (1987).
15. A.K. Bhattacharya and W.D. Nix, Int. J. Solids Structures **24**, 1287 (1988).
16. T.Y. Tsui, C.A. Ross, and G.M. Pharr, Mater. Res. Soc. Symp. Proc., in press.
17. T.Y. Tsui, C.A. Ross, and G.M. Pharr, Mater. Res. Soc. Symp. Proc., in press.
18. T.Y. Tsui, W.C. Oliver, and G.M. Pharr, J. Mater. Res. **11**, (1996).
19. A. Bolshakov, W.C. Oliver, and G.M. Pharr, J. Mater. Res. **11**, (1996).
20. A. Bolshakov, W.C. Oliver, and G.M. Pharr, Mater. Res. Soc. Symp. Proc. **436**, 141 (1997).
21. A. Bolshakov and G.M. Pharr, J. Mater. Res., submitted.
22. I.N. Sneddon, Int. J. Engng. Sci. **3**, 47 (1965).
23. T.Y. Tsui, Ph.D. Dissertation, Rice University, 1996.
24. T.Y. Tsui and G.M. Pharr, J. Mater. Res., submitted.
25. K.L. Johnson, Contact Mechanics (Cambridge University Press, Cambridge, 1985).